"Defects in Microelectronic Materials and Devices"
Edited by Daniel Fleetwood, Sokrates Pantolides, and Ronald D. Schrimpf
Published by CRC Press, 2008 ISBN 1420043765
Chapter 11, pp 341-358

11

Defects in CMOS Gate Dielectrics

Eric Garfunkel, Jacob Gavartin, and Gennadi Bersuker

CONTENTS

11.1 Introduction 341
11.2 Theoretical Approaches to Understand Dielectric Defects 343
11.3 Physical Methods of Defect Detection in Dielectrics 348
11.4 Electrical Methods of Defect Characterization 351
References 355

11.1 Introduction

The electrical and optical behavior of semiconducting devices is often dominated by the quantity, energy, and physical location of defects. Five decades of research on Si-based devices have led to a reasonable (although not definitive) consensus concerning the nature of defects in complementary metal-oxide semiconductor (CMOS) gate stack dielectrics [1–3]. This understanding has resulted from a continuous interplay between theoretical computation of model structures and experimental measurements of films and devices using a variety of methods. Some of the defects involve changes in local structure or stoichiometry. For example, a slight excess of Si atoms in an otherwise perfect SiO_2 film will result in the appearance of Si–Si bonds. These bonds result in electronic states in the SiO_2 band gap that can become charged under certain conditions. Other defects involve dangling bonds, either at the Si/SiO_2 interface or in the bulk of the SiO_2 film. A third class of defect involves changes in local coordination (Si becoming three- or fivefold coordinated, or O becoming threefold coordinated). Yet another class involves impurity atoms in the film, hydrogen being predominant. Although most impurities degrade device performance, hydrogen can also improve device properties when present at appropriate concentrations and in the appropriate location (usually by bonding with uncoordinated/dangling bonds). The role of nitrogen incorporation into these films as industry has moved from SiO_2 to SiON dielectrics has been extensively studied [2]. Finally, the role of radiation damage in dielectrics has also received much attention over the past few decades, especially for space and some military applications.

Over the past few years, a new class of dielectrics with higher permittivity than SiO_2 or SiON has appeared in the gate stack of CMOS devices. The first new gate dielectric is hafnium oxide based, as hafnia has an optimal combination of properties, including being quite stable against reduction when integrated onto a silicon channel-based platform [4–6].

During the exploration of HfO_2 and other high-permittivity metal oxide gate dielectrics over the past decade, the critical issue of the nature, quantity, energy, and electrical behavior of defects has come to the fore. As with SiO_2-based dielectrics, defects again are thought to involve nonideal stoichiometry, structural imperfections, and impurities. Current thinking by many experts is that O vacancies are a predominant cause of defects. We spend some time in this review outlining our understanding of this class of defects, including presenting recent results of ab initio based calculations of the energies of the various defects.

In most cases currently being explored, the gate stacks formed using Hf oxide and Hf silicate thin films represent multilayer structures that include a SiO_2 layer intentionally or spontaneously formed at the interface with the substrate. This interfacial SiO_2 layer may be nonuniform across its thickness due to its interaction with the high-*K* film [7]. Defects in both high-*K* and interfacial layers are believed to affect device electrical characteristics, although the nature and concentration of each set is still a matter of debate. Hydrogen has also been implicated in both enhancing and passivating defects in high-*K* oxides. Finally, nitrogen may appear in high-*K* gate stacks primarily as a structural/thermal/chemical-stabilizing species, rather than directly enhancing the device electrical properties (as it does in current generation SiON structures).

As industry and the research community progress in their understanding of high-*K* integration, control of the various defects and mitigation of the negative electrical consequence of defects will continue to be aggressively pursued. The understanding that is coming from high-*K* on Si studies also helps the field as it moves from Si to higher mobility substrates such as Ge and III–V materials. Given the higher relative concentration of electrical defects in metal oxides that have been observed in most studies to date, there is also concern that radiation effects could become an even more serious problem with high-*K* oxide gate stacks than similar SiO_2-based ones.

In this chapter, we briefly review selected experimental measurements and computational calculations of defects in HfO_2-based CMOS gate stacks. From one perspective, defects in the dielectric can be viewed as structural and/or compositional anomalies (vacancies, impurities, multiple phases, etc.). There are several classes of possible defects in the HfO_2/SiO_2 stack, for example: (1) vacancies—O, Hf, or Si; (2) impurities—H, Si, Ti, Zr, Hf, N, C, Cl, F, etc.; (3) interstitials—O, Hf, and Si; and (4) various combinations of (1)–(3). At the same time, the defects can be classified by their origins: thermodynamic defects whose concentrations are defined solely by their free energies of formation, and kinetic defects, whose concentration and distribution are metastable, process dependent and, to some extent controllable. Moreover, as the thermodynamic conditions in the dielectric stack vary during the device operation, the concentration and distribution of thermodynamic and kinetic defects may also evolve reversibly or irreversibly.

We also discuss the electronic structure of proposed defects, including their densities and charge state (if any) in the dielectrics (and at the interfaces). And from yet another vantage, we discuss how defects affect various electrical properties of the gate stack, such as leakage current, band alignment, charge trapping, threshold voltage, mobility, reliability, etc.

The chapter is organized as follows. In Section 11.2, we present theoretical models of defects. In Section 11.3, we review some of the experimental results of physical measurements (most involving different forms of spectroscopy). In Section 11.4, we evaluate electrical measurements that have been performed in our labs and elsewhere. There are still some uncertainties in our understanding of defects; however, the agreements between theory and experiment are tantalizing. Finally, we speculate on how these defects will respond to radiation based on initial results and understanding in the field.

11.2 Theoretical Approaches to Understand Dielectric Defects

With regard to defects in a gate stack, atomistic theories have a dual aim:

1. *Explorational*. Given the materials composition, identify most likely (energetically favorable) structural defects and evaluate their thermodynamic properties such as free energies of formation, migration and aggregation, ionization energies, and electron affinities.
2. *Metrological*. Calculate measurable characteristics of defects such as local structure, vibrational frequencies and their activities, electronic energy levels and corresponding optical absorption spectra, electronic spin resonance (ESR) parameters, effective cross sections for charge trapping, chemical shifts for x-ray spectroscopy, etc.

Although present state-of-the-art ab initio calculations allow for evaluation of many properties listed above, none of the existing methods are capable of doing this with high accuracy for all of the properties. The atomistic modeling approaches can be classified by their three main components: the Hamiltonian (Hartree–Fock and post Hartree–Fock, various approximations to density functional theory (DFT), etc.), the basis set (plane waves, atomic orbitals, numeric), and the boundary conditions (periodic, finite cluster, or embedded cluster). These three components may be realized in various combinations. The merits and limitations of various techniques are discussed in many textbooks and reviews (see Ref. [8]).

The most widely used approach is the plane wave density functional (PW-DFT) method utilizing various pseudopotential approaches to treat core electrons and the Kohn–Sham approximation to DFT, and periodic boundary conditions. The PW-DFT method is implemented in many software packages such as VASP [9], CASTEP [10], ABINIT [11], and CPMD [12] to name a few. The PW-DFT approach combines relative simplicity and accuracy and has been proven effective for reliable structural and vibrational information. However, its main well-documented limitation is a severe underestimation of the single-particle band gaps of insulators and semiconductors, and defect level splittings from the band edges. This seriously limits the reliability and accuracy of direct calculations of band alignment at the dielectric/semiconductor and dielectric/metal interfaces [13–15] and optical and electrical properties of defects [16,17]. The band gap problem can be resolved by lifting the local or semilocal approximation to the exchange energy functional in local (LDA) and generalised gradient (GGA) corrected functionals. Several existing methods such as the GW approximation [18], time-dependent DFT [19], screened exchange (sX) [20], and self-interaction correction (SIC) [21] have been used, but their merits and limitations still must be validated. The complexity of these approaches severely restricts the size of the systems that can be calculated and the possibility of structure optimization. An alternative, more economical, but also more empirical approach is to use hybrid functionals in conjunction with plane waves (PBE0 functional [22] and CPMD package [12]) or local orbitals (B3LYP functional [23] and CRYSTAL03 package [24]). The applicability of hybrid functionals has been tested on numerous oxide systems [25].

As noted above, a likely culprit behind one or more of the dielectric defects is the oxygen vacancy. We suspect this for several reasons: among other things, oxygen and hydrogen anneals have a significant effect on the charge in the dielectric that is measured electrically, and perovskite oxides are notorious for having oxygen vacancies (quite useful for oxygen transport in this class of materials). So, what is the argument making oxygen vacancies a most likely defect? First, consider an oxygen vacancy–interstitial pair of defects (Frenkel pair V^{q}–O_{i}^{-q}) in monoclinic hafnia (m-HfO_2). The calculated formation energies $E_{Fr}(q)$ are

8.1, 7.0, and 5.6 eV for charges $q=0$, 1, 2, respectively, strongly suggesting the V^{2+}–O^{2-} combination to be the most stable [16,26]. Once created, oxygen interstitials are found to be extremely mobile even at room temperature [27]. Therefore, oxygen diffusion out of the dielectric into either the metal or the substrate is possible. Reaction of the interstitial with the substrate or metal is also quite exothermic (for most relevant materials). For example, oxidation of the Si–Si bond in the substrate is favorable with respect to oxygen interstitials in m-HfO_2 by ~3–4 eV [28]. Thus, the extended Frenkel pair of a vacancy in HfO_2 and oxygen in Si has a formation energy of only 1.6–2.6 eV. Similar studies of oxygen exchange between HfO_2 and various metal gates [29] also found reduction of formation energies in the extended Frenkel pairs. Therefore, hafnium-based thin films have a propensity for oxygen to escape to a semiconducting substrate or a metal gate, leaving excess oxygen vacancies in the dielectric. However, the sizable positive defect formation energies suggest that this process is technically suppressible (e.g., by interface nitridation).

Numerous earlier calculations of isolated oxygen vacancies in HfO_2 were based on PW DFT and Kohn–Sham approaches using LDA or GGA approximations (see Refs. [8,17,26]). These calculations predicted three stable charge states for oxygen vacancies in various polymorphs of HfO_2—V^{2+}, V^{+}, and V^{0}. Calculated electrical levels associated with thermodynamic charge switching between various charge states of the vacancy were predicted in the mid gap region of HfO_2, and thus, also in the Si gap region in the Si/HfO_2 stack. However, this result was in conflict with electrical measurements placing the energies of electron traps in the conduction band offset region of Si/HfO_2. This discrepancy prompted suggestions of alternative shallow trap candidates. For example, various forms of oxygen interstitials were considered [15,16,26,27], and impurity-induced states from H and Zr were discussed by Shluger et al. [8] and Bersuker et al. [7]. Nevertheless, the almost universally observed sensitivity of trap density to oxygen exposure during and after high-K film deposition, and the much weaker dependency on the metallic precursors, strongly points to oxygen deficiency related defects.

This controversy was resolved in recent atomistic studies that revealed that one key vacancy in HfO_2 is an amphoteric defect, i.e., it may accept negative as well as positive charge. Although the existence of negative oxygen vacancies was first suggested from the GGA calculations [7], the obtained trapping energies were far too small. More refined treatment of the electron exchange interaction was necessary for accurate predictions. Negative oxygen vacancies were later predicted using sX approximations [15,30], hybrid density functional [31–33], and the SIC approximation [34].

The results of these different calculations are qualitatively similar, although the numerical differences and accuracies of these approaches warrant separate comparative analysis, as seen below. Here, we follow results [32,33] obtained for monoclinic HfO_2 using atomic basis sets and nonlocal B3LYP density functional [23] as implemented in the CRYSTAL03 package [24]. The single-particle energy diagram for various charge states of a four-coordinated oxygen vacancy is schematically depicted in Figure 11.1. The calculated single-particle band gap of the monoclinic (m)-HfO_2 is about 6.1 eV, i.e., slightly larger than is experimentally observed, 5.6–5.9 eV [35], although there remains some uncertainty in the experimental value as well. As discussed before, oxygen vacancies in m-HfO_2 may exist in five charge states +2, +1, 0, −1, −2, with up to four extra electrons in the vicinity of the vacant O^{2-} site. This property is truly surprising: an ability of a defect to act both as a donor and an acceptor is well established in nonpolar covalent systems (e.g., a single vacancy in Si [36]), but is unexpected in polar wide-gap dielectrics. Interestingly, the preferred oxygen vacancy site in m-HfO_2 depends on the charge state: V^{2+} and V^{+} are more stable in threefold coordinated sites, whereas the V^{0}, V^{-}, and V^{2-} states are energetically more favorable at the fourfold coordinated sites. However, the difference in

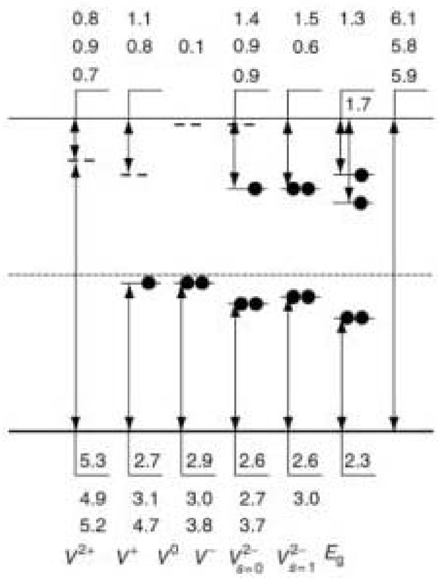

FIGURE 11.1
One-electron level diagram for oxygen vacancies in monoclinic and cubic HfO_2 calculated using different approaches. At the top and bottom of the figure, the first row refers to periodic calculations with an atomic basis set, a B3LYP density functional and a 96 atoms supercell (From Gavartin, J.L. et al., *Appl. Phys. Lett.*, 89, 082908, 2006; Ramo, D.M. et al., *Phys. Rev. B*, 75, 205336, 2007); the second row refers to PW-DFT calculations with an RPBE0 density functional and a similar supercell (From Broquist, P. and Pasquarello, A., *Appl. Phys. Lett.*, 89, 262904, 2006); the third row refers to PW-DFT calculations with an sX density functional and a cubic supercell of 54 atoms. (From Robertson, J., *Rep. Prog. Phys.*, 69, 327, 2006; Xiong, K. et al., *Appl. Phys. Lett.*, 87, 183505, 2005.)

formation energies for doubly negatively charged vacancies between three- and four-coordinated sites is only about 0.2 eV.

The change of the charge state of the vacancy (trapping and detrapping) is associated with a large local lattice relaxation associated with polarization energies in the range of 0.5–1.0 eV. The direct consequences are an asymmetry in charge trapping and detrapping kinetics and differences in characteristic energies as observed in optical (reflection ellipsometry, adsorption, and photoluminescence) and electrical (*I–V* and *C–V*) probes. The difference between optical and thermal ionization of defects has been extensively discussed in the literature (see Ref. [37]), and can be qualitatively explained by the potential surface diagram depicted in Figure 11.2. Optical ionization occurs at time scales much faster than characteristic lattice vibrations. Thus, an electronic transition from the trap of charge q (state A) onto the conduction band minimum (CBM) (state B*) can be considered in a frozen lattice, which corresponds to a Frank–Condon type vertical transition E_{opt}. However, the ionized trap induces lattice polarization, which in the case of the oxygen vacancy is mainly associated with the outwards displacement of the nearest neighbor Hf ions. This relaxation coordinate is denoted as Q in the diagram. The minimum energy state B corresponds to a fully relaxed trap state $q-1$, and the electron is delocalized at the CBM. Thermal ionization of the trap is a slow phonon-assisted process with the activation energy E_{th}.

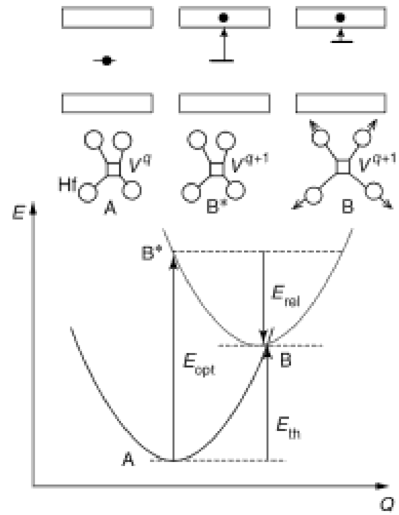

FIGURE 11.2
Schematic potential energy surface for optical and thermal detrapping processes. Generalized displacement of the nearest neighbor Hf ions, Q, is shown, and the energy scale is chosen to represent ionization of V^{2-} vacancy. The band diagram schematically illustrates optical and thermal ionization processes, respectively, without (B*) and with (B) lattice relaxation. (After Gavartin, J.L. et al., *Appl. Phys. Lett.*, 89, 082908, 2006. With permission.)

By construction of Figure 11.2, E_{th} may be approximated as

$$E_{th} = E_{opt} - E_{rel}. \tag{11.1}$$

Optical and thermal ionization energies can be deduced as a combination of the calculated total energies of different systems as follows:

$$E_{opt}(V^q) = E_q(V^{q+1}) - E_q(V^q) + E^- - E^0, \tag{11.2}$$

$$E_{rel}(V^{q+1}) = E_{q+1}(V^{q+1}) - E_q(V^{q+1}), \tag{11.3}$$

where
E^0 is the total energy of the perfect HfO_2 crystal
E^- is the total energy of the perfect HfO_2 crystal with an electron at the bottom of the conduction band
$E_q(V^q)$ is the total energy of HfO_2 with the vacancy in a charge state q ($q = +2$, $+1$, 0, -1, -2) in the optimized geometry
$E_q(V^{q+1})$ is the total energy of the vacancy in the charge state $q+1$ but at the equilibrium geometry corresponding to the vacancy in the charge state q

The calculated optical excitation energies from the defect states into the CBM and the thermal detrapping energies of oxygen vacancies are summarized in Table 11.1. The defect energies, especially for the shallow defects, critically depend on the nonlocal exchange interaction method used. Most of the existing approaches are based on so-called hybrid functionals in which the local or GGA exchange functional is mixed with the Hartree–Fock exchange using one or another empirical scheme. Although these

TABLE 11.1

Optical Excitation Energies, E_{opt}, Relaxation Energies, E_{rel}, and Thermal Activation Energies, E_{th}, for Oxygen Vacancies in m-HfO_2 Calculated Using Equations 11.1 through 11.3

Charge	E_{opt} (eV)	E_{rel} (eV)	E_{th} (eV)
V^+	3.33	1.01	2.32
V^0	3.13	0.80	2.33
V^-	1.24	0.48	0.76
V^{2-}	0.99	0.43	0.56

Source: After Gavartin, J.L. et al., *Appl. Phys. Lett.*, 89, 082908, 2006. With permission.

approaches seem relatively accurate in general, the error margins associated with specific systems are essentially unknown. Therefore, it is instructive to compare the results obtained using different methods.

Comparisons of the B3LYP calculations [32,33] with PBE0 [31] and sX [15,30] indicate an agreement within 0.3–0.4 eV in most of the single-particle energies with respect to the band edges (Figure 11.1). Most of the discrepancies may be attributed to different single-particle band gap energies predicted in these approaches. As noted above, the B3LYP method predicts the largest one-electron band gap with the largest deviation from E_g measured by optical absorption (~5.6 eV [34]). However, single-electron estimates of band gaps neglect excitonic effects and the effects of phonon broadening, which may reduce the measured optical band gap of HfO_2 by up to 0.8 eV [38]. Similar arguments apply to the adsorption energies associated with optical transitions between the valence band and V^{2+} level. An apparent close agreement of the calculations [31] with the reflection ellipsometry measurements [39] is somewhat deceptive. Single-particle calculations do not include electron–hole interaction, which is significant for such transitions. When taken into account (say using the TDDFT method and M3LYP functional), this interaction reduces the transition energy to 4.9 eV, that is, ~0.5 eV lower than the single-particle energy difference [33], bringing it closer to experiment. Apparently, the positive and negative oxygen vacancy interplay is not unique for HfO_2. Recent atomistic studies predict similar behavior in tetragonal hafnium and zirconium silicates [40–42], and even in silica [43]. However, no experimental confirmation has yet been reported for negative vacancy states in either silica, hafnon ($HfSiO_4$), or zircon ($ZrSiO_4$) to the best of our knowledge.

An important feature of the optical signal associated with the oxygen deficiency in HfO_2 is that its width strongly increases with vacancy concentration [39]. This issue has been studied theoretically using the PW-DFT approach and a GGA energy functional [44]. First, it was concluded that oxygen divacancies, although not energetically favorable, may form under certain conditions (with near zero-binding energy). Second, the case of multiple vacancies was considered in a large supercell of 324 atoms. It was demonstrated that, by a 5% vacancy concentration, the vacancy signal significantly broadens. This effect is illustrated in the time evolution of the one-electron levels calculated using Born–Oppenheimer molecular dynamics (Figure 11.3). Remarkably, even at room temperature the dynamical fluctuations of localized defect and band edge levels occur on a scale much larger than the thermal energy. This gives rise to a broad (>1.5 eV) defect band and long band tails, which are also observed in reflection ellipsometry of oxygen-deficient films [39]. The static lattice relaxation near the isolated neutral vacancy is negligible, so the strong interaction between the separated vacancies is yet another manifestation of a strong electron–lattice coupling in high-*K* systems [45]. Another phenomenon associated with strong electron–phonon coupling is the possibility of small polaron formation; these are electronic states localized by

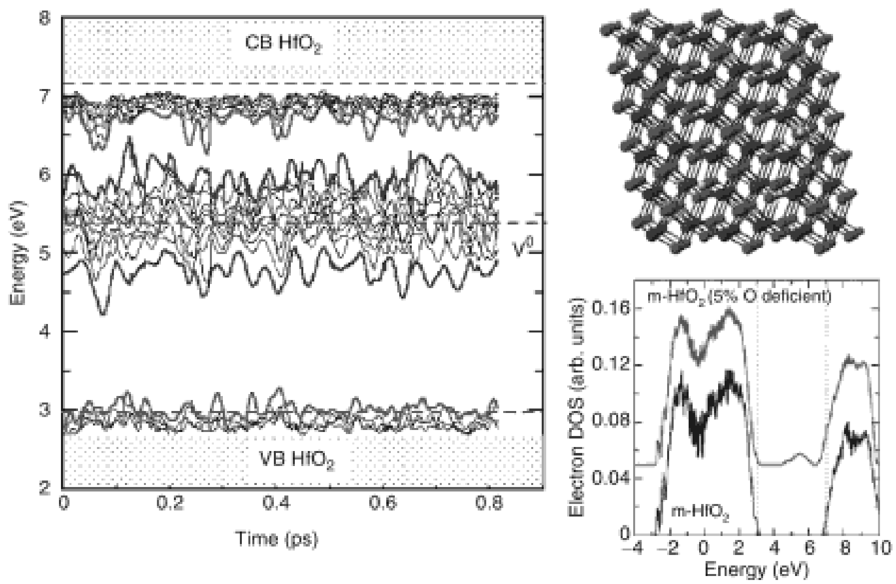

FIGURE 11.3
Dynamics of the one-electron levels of m-HfO_2 with ~5% neutral oxygen vacancies calculated in a supercell of 324 ions using Born–Oppenheimer MD at $T = 300$ K. The positions of the band edges and a single vacancy level in a static calculation are shown as dashed lines. The resulting electron DOS is shown in comparison with a perfect m-HfO_2 at the same temperature. (After Gavartin, J.L., et al., *Physics and Technology of High-K Dielectrics*, 4, Kar, S., et al., Eds., *Electro Chemical Society*, Pennington, New Jersey, 2006, p. 227. With permission.)

lattice polarization, induced by the carriers themselves. The negative oxygen vacancy is one example of a small polaron [46]. The possibility of electron and hole self-trapping was also suggested in amorphous HfO_2 films [44,46] and even in perfect monoclinic hafnia [47,48]. Small polarons in high-*K* dielectrics may have a significant contribution to the trapping kinetics, leakage currents, defect formation, and film degradation. It is also a challenging problem for atomistic modeling, and currently is a subject of intensive research.

11.3 Physical Methods of Defect Detection in Dielectrics

In this section, we briefly review two classes of "nonelectrical" experimental dielectric defect analysis methods—one microscopic and the other spectroscopic. We note ESR work in the final "electrical methods" section. There are other tools that have been used to help elucidate defect behavior that we have not reviewed here, including Fourier transform infrared (FTIR) [49–51] and cathodoluminescence [52].

Imaging defects in HfO_2 dielectrics has proven a difficult task. Surface defects, as can be seen in scanning probe microscopy, are unlikely to be the same as defects in the bulk. Electron microscopy is also difficult at the single defect level; it is virtually impossible to imagine seeing a single oxygen vacancy in a SiO_2 or HfO_2 film. One exception is that of imaging heavy Z atoms (e.g., Au or Hf) in a light Z matrix (e.g., C or even SiO_2), which makes seeing a Hf atom in an SiO_2 interfacial layer possible [53]. On the other hand, oxygen deficiencies in the interfacial SiO_2 layer may manifest themselves in other

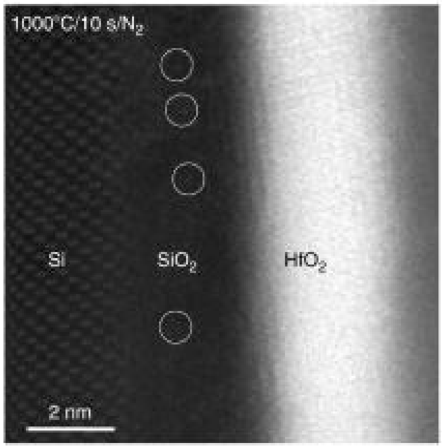

FIGURE 11.4
ADF TEM image of a 3 nm HfO_2/2 nm SiO_2/Si stack after a 1000°C anneal. Stray Hf atoms in the IL are circled. (From Bersuker, G., et al., *J. Appl. Phys.*, 100, 09418, 2006. With permission.)

spectroscopic ways, including via their spectral features corresponding to under-coordinated Si atoms as observed in the Si $L_{2,3}$ electron energy loss spectra (EELS). In Figure 11.4, we show a transmission electron microscopy (TEM) image of a high-*K* gate stack fabricated with a 2 nm thermal SiO_2 interfacial layer followed by 3 nm ALD HfO_2 film. After the stack was exposed to a 1000°C/10 s anneal, isolated Hf atoms, in the density range of 10^{12} to 10^{13} cm^{-2}, were found in the SiO_2 layer. At the same time, the high-temperature anneal resulted in significant oxygen deficiency of this interfacial layer, as demonstrated by the rise of the shoulder associated with the under-oxidized Si atoms in the EELS spectra (Figure 11.5).

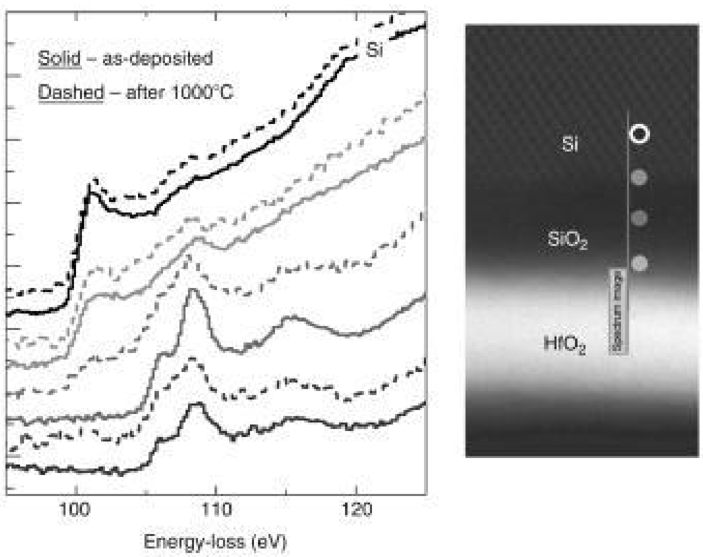

FIGURE 11.5
ADF TEM image and Si $L_{2,3}$ edge EELS taken at the identified positions in the 3 nm HfO_2/2 nm SiO_2 stack before (a) and after (b) anneal. (From Bersuker, G., et al., *J. Appl. Phys.*, 100, 09418, 2006. With permission.)

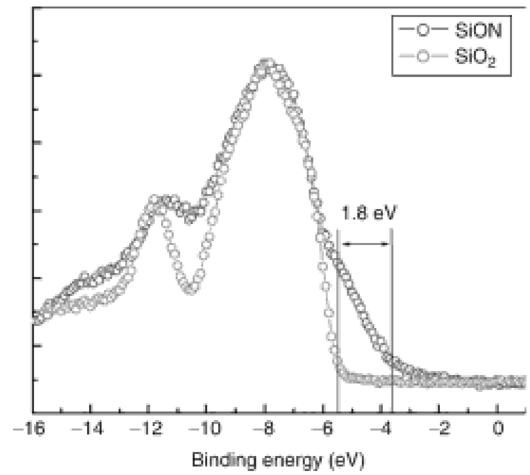

FIGURE 11.6
PES (taken at Brookhaven) of HfSiO/Si and HfSiNO/Si ultrathin films. Note especially the difference in top of the valence band. (From Sayan, S., et al., *Appl. Phys. Lett.*, 87, 212905, 2005. With permission.)

Variants of photoemission spectroscopy (PES) have also been employed to examine defects in dielectrics. One set of photoemission methods focuses on developing an accurate picture of the density of states (DOS) in the valence band. The spectra of two $HfSiO_x$ systems, one with and one without nitrogen present, are shown in Figure 11.6 [54]. The incorporation of nitrogen leads to a significant DOS at the top of the valence band, which in the pure oxides (hafnium and/or silicon oxide) is predominantly of O 2p character. Whether nitrogen can be called a defect or not is mainly a semantic issue; it is clear that it results in a significant DOS at the bottom of the gap (at the top of the valence band). A second, related method is called inverse photoemission (InvPES). In InvPES, electrons with an energy of order 20 eV impinge upon a surface, fall into unoccupied levels, and emit a photon with an energy given by the difference between the incident kinetic energy and energy of the state into which they fall. As the probability for photon emission is directly related to the density of unoccupied states into which the electrons fall, the InvPES spectrum roughly maps out the density of unoccupied states within the first 10 eV of the Fermi energy. In Figure 11.7, we present an InvPES spectrum from a HfO_2/Si sample. In the same figure, we also plot out an ultraviolet light excited photoemission (UPS) spectrum (occupied DOS) taken on the same sample in the same

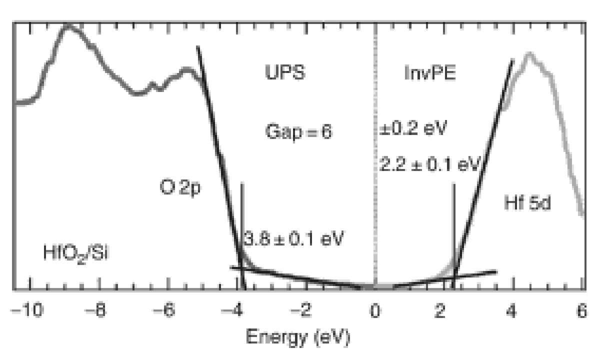

FIGURE 11.7
UPS and InvPES of a 2 nm HfO_2 film on Si. The densities of states relative to the Fermi level ($E = 0$) and the gap can readily be observed. Defects and band tail states are also sometimes observed. (From Bartynski, Garfunkel, et al., previously unpublished data.)

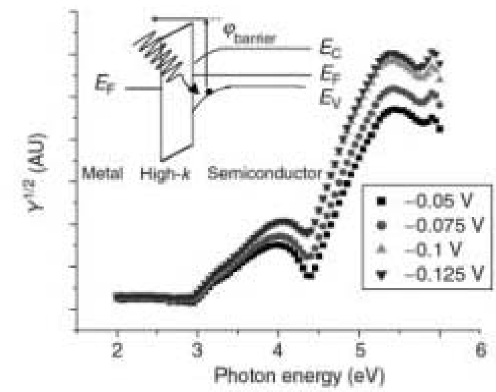

FIGURE 11.8
IntPES spectra from a Al/HfO_2/Ge gate stack. HfO_2 (conduction band) to Ge (valence band) energy offset measured to be ~3.1 eV. (From Garfunkel and Celik, previously unpublished data.) Energies listed in box refer to bias across MIS structure.

chamber on the same day. Although very useful for getting a big picture of the major components of the system's electronic structure, PES and InvPES are not particularly useful for determining the electronic structure of defects that may be present in the system at a level that is much less than 1% of the total atomic density.

Two more variants of photoemission that yield very helpful information about the system's electronic structure are internal photoemission (IntPES—see especially the extensive work of Afanas'ev and Stesmans [55,56] and x-ray photoelectron (XPS) energy loss spectroscopy, and total photoelectron yield spectroscopy (especially the work of Miyazaki, Hirose, et al. [57,58]). IntPES is performed by shining monochromatic light onto an ultrathin capacitor structure (metal–insulator–metal [MIM] or metal–insulator–semiconductor [MIS]) and measuring the photoinduced current as a function of photon energy, bias across the insulator, sample and processing conditions, etc. Some believe that this is an accurate way to both determine band edge energies and to observe states in the gap. As the photocurrent yield axis is not linear (following standard practice in the field), low density defects are enhanced. In Figure 11.8, we present one set of our IntPES results from a study of various substrates and metal gates sandwiching a HfO_2 dielectric. One result relevant to defect characterization is the appearance of band tail states near the top of the gap on samples that also show a high electrical defect concentration.

Another set of experimental measurements that yields information about defects comes from optical spectroscopy. The idea is that the cross section for optical absorption comes only when there is an unoccupied state present that can accept an electron. There are various ways to examine this, one being ellipsometry [51,59]. In ellipsometry a plot of the imaginary part of the dielectric function versus energy is loosely related to the density of unoccupied states. In Figure 11.9, we show the imaginary part of the dielectric function for two hafnium silicates (the same sample set as presented in Figure 11.6) [54]. Clearly the gap narrows when nitrogen is included in the dielectric. It is not clear from these data alone whether that narrowing arises because of states at the top or bottom of the gap—here PES and InvPES offer a more complete picture of the DOS changes. The optical-based methods of characterization such as IntPES, ellipsometry, and cathodoluminescence are usually more sensitive to lower defect concentrations.

11.4 Electrical Methods of Defect Characterization

Electrical characterization allows one to identify electrically active defects relevant to device performance with exceptional sensitivity, on the order of 10^{10} cm^{-2}. This level

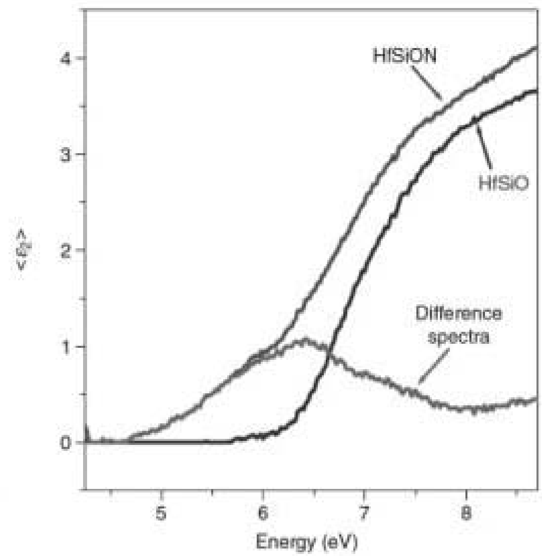

FIGURE 11.9
The imaginary part of the dielectric function for two hafnium silicates, and the difference spectrum, showing how N narrows the effective gap. (After Sayan, S., et al., *Appl. Phys. Lett.*, 87, 212905, 2005. With permission.)

of sensitivity, developed over several decades as devices have scaled from the micron to nanometer regime, is much higher than can be realized with most "physical" methods (e.g., PES, TEM, FTIR, ion scattering, ellipsometry, etc.). Gate stacks formed using hafnium oxide and hafnium silicate thin films currently being considered for gate dielectric applications represent multilayer structures that include an SiO_2 layer formed at the interface with the substrate [60]. The high density of the as-grown electron/hole traps found to be present in the high-K dielectric stacks may dramatically degrade transistor performance due to very fast charge trapping processes (in the μs range) to which they can contribute. Specific electrical techniques with good spatial (especially depth) and time resolution are then required to probe electrically active defects either in the high-K or interfacial SiO_2 layers. In particular, during pulsed I_d–V_g measurements on nMOSFETs [61], some electrons injected from the transistor inversion layer into the dielectric during nanosecond–microsecond pulses applied to the gate become trapped in as-grown defects in the HfO_2 film. This type of measurement results in well-localized (from the dielectric thickness standpoint) trapped charges, since trapping of the tunneling electrons proceeds most effectively via a resonant process [62], while short pulse time prevents redistribution of the trapped charges between the adjacent traps. By subtracting contributions due to the fast resonant trapping from the total threshold voltage shift after long-term stress, one can obtain an electrical signature of the slow charge redistribution process (process B in Figure 11.10), and use it for extraction of the trap energies. Fitting results for all voltages in the whole temperature range yields trap energies on the order of 0.35 and 0.45 eV below the conduction band edge. This value is consistent with calculated energies of the single and double charged negative oxygen vacancies in monoclinic hafnia [31,32]. Measured and modeled trapping effects on V_t are shown in Figure 11.11.

Interfacial SiO_2 layers in high-K gate stacks can be profiled using frequency-dependent charge pumping techniques. The frequency dependence can be converted into a distance (across the dielectric) dependence [63]. Trap generation in the interlayer (IL), ΔN_{it}, is higher close to the high-K layer, while in the gate stacks with different IL thicknesses, $N_{it}(x)$ values in the IL are similar at the same distance x from the high-K film, Figure 11.12 (here N_{it} is plotted against the distance from the HfO_2/SiO_2 interface) [64]. At the same time, the rate

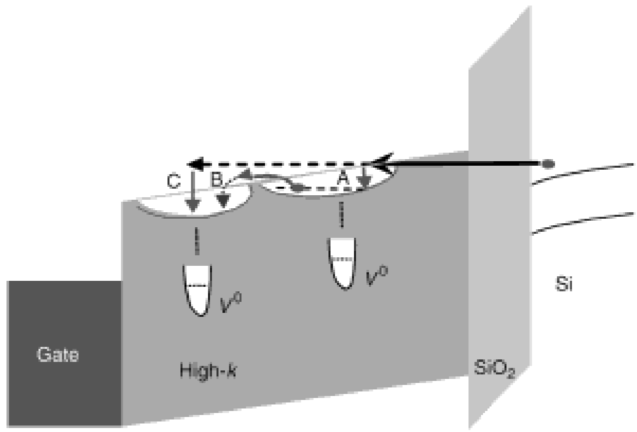

FIGURE 11.10
Schematic diagram of the electron trapping processes: A—electrons injection from the conduction band and trapping at a shallow defect (presumably neutral O-vacancy (V^0)), which leads to the formation of a negative O-vacancy accompanied by lattice relaxation (down arrow); B—a temperature-assisted electron detrapping/retrapping; Process C is ineffective due to the mismatch of the electron and trap energies. (From Bersuker, G., et al., *Proc. IEEE Intl. Reliab. Phys. Sympos.*, 2006, p. 179. With permission.)

of trap generation in the IL, $R_{it}(t) = \Delta N_{it}(t + \Delta t)/\Delta t$, decreases with the stress time, t, along with the stress-induced leakage current (SILC) (Chapters 15 through 17) generation rate, $R_{SILC}(t)$, in Figure 11.13.

Similar growth rates of SILC and N_{it} suggest that their increase is most likely driven by the same defects within the IL. The decrease in the degradation rate with time, Figure 11.13, indicates that the electron traps are generated in the IL at preexisting, precursor defect sites, whose density increases closer to the high-K film. That they exist prior to electrical stressing suggests that these precursor defects could be induced by the interaction of the IL with the high-K dielectric. Recent physical results (scanning tunneling electron microscopy (STEM)/EELS, ESR, XPS, ion scattering) strongly suggest that the Hf-based high-K films modify the stoichiometry of the underlying SiO_2 layer by rendering

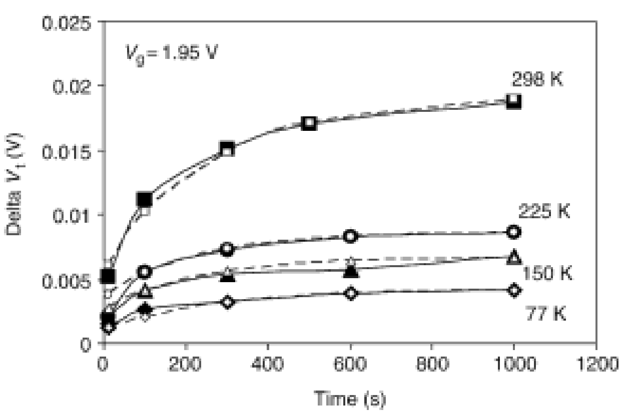

FIGURE 11.11
Measured and modeled (open symbols) V_t shift associated with the slow trapping process (A) of Figure 11.10 during the $V_g = 1.95$ V stress at different temperatures. (From Bersuker, G., et al., *Proc. IEEE Intl. Reliab. Phys. Sympos.*, 2006, p. 179. With permission.)

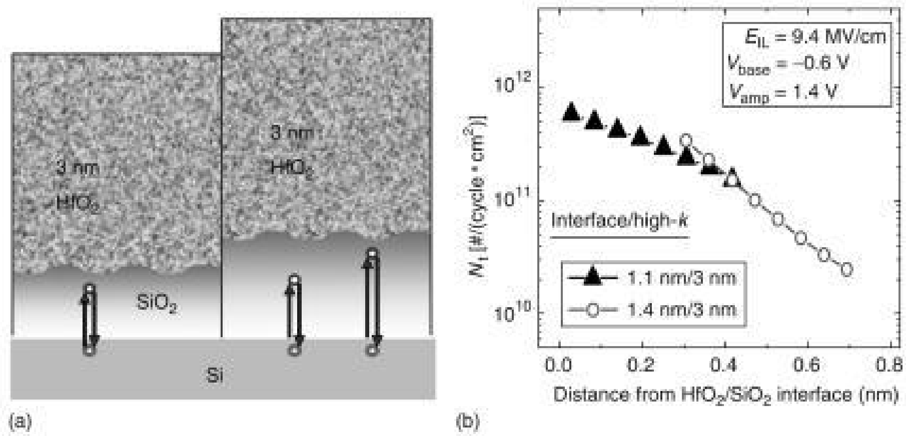

FIGURE 11.12
Simple schematic diagram (a) of the electron probing of the traps during charge pumping measurements, and (b) N_{it} plotted versus the distance from the HfO_2/SiO_2 interface. (After Young, C.D., et al., *IEEE Trans. Dev. Mater. Reliab.*, 6, 123, 2006. With permission.)

it oxygen-deficient. Precursor defects associated with the oxygen vacancies (for instance, Si–Si defects) can be converted into electron traps during stress (by breaking the Si–Si bonds), giving rise to SILC.

The electrically detected ESR technique called spin-dependent recombination (SDR), has several orders of magnitude greater sensitivity than "conventional" electron spin resonance (Chapter 6) and allows measurements in fully processed transistors [65].

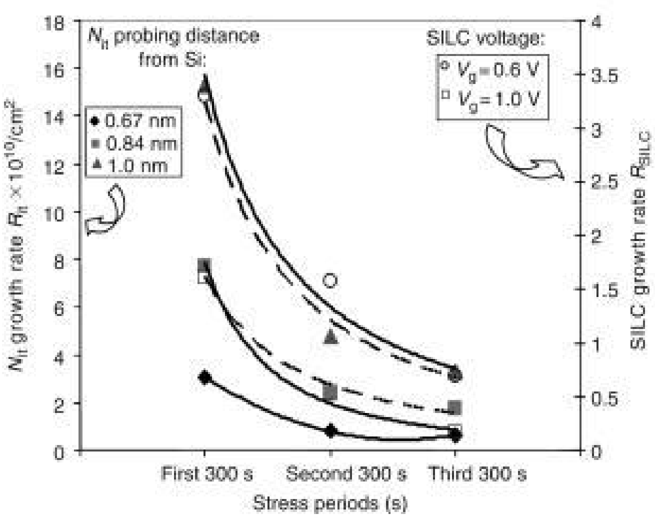

FIGURE 11.13
SILC and trap generation rates obtained by averaging the SILC and N_{it} growth over the subsequent 300 s stress intervals at different distances from the Si substrate and different SILC voltages, respectively, under a low-voltage CVS ($V_g = 2.4$ V). Trends for the trap generation and SILC rates are shown by solid and broken lines, respectively.

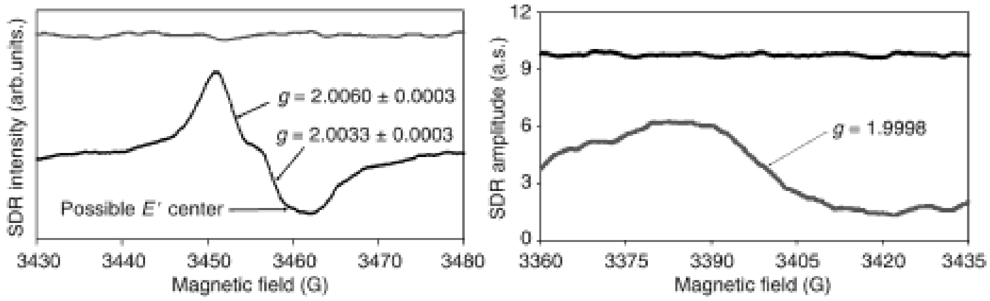

FIGURE 11.14
SDR signal measured on a $HfO_2/SiO_2/Si$ stack. (After Neugroschel, A., et al., *IEEE IEDM*, 2006, p. 137. With permission.)

By simultaneously exposing a device, appropriately biased (for maximum recombination), to a large magnetic field and microwave irradiation, one can observe the magnetic resonance response of deep level recombination centers by monitoring the response of the recombination current versus magnetic field. SDR measurements performed on high-*K* transistors show a new signal after the initial few seconds of stress, which is not observed in the SiO_2 stack, Figure 11.14 [66]. Due to the broadness of this signal, indicative of the presence of d-type electronic states, the additional defects can tentatively be assigned to Hf atoms, which were found to be present in low concentrations ($\sim 10^{13}/cm^2$) in the interfacial SiO_2 layer (Figure 11.4).

Research on the effects of radiation on high-*K* devices is still in its initial phase [67–76]. In an ionizing radiation environment, SiO_2-based MOSFETs are known to predominantly trap holes with some electron trapping being observed due to the existence of neutral electron traps or new electron trap creation in the oxides. The presence of the interfacial SiO_2 layer in the high-*K* gate stack suggests that one may expect an electrical response similar to that of a very thin SiO_2 film, although significantly amplified by the SiO_2 interaction with the high-*K* film. Studies of radiation effects in high-*K* stacks are ongoing.

References

1. Buchanan, D.A., Scaling the gate dielectric: Materials, integration, and reliability, *IBM J. Res. Dev.*, 43, 245, 1999.
2. Green, M.L. et al., Ultrathin (<4 nm) SiO_2 and Si–O–N gate dielectric layers for silicon microelectronics: Understanding the processing, structure, and physical and electrical limits, *J. Appl. Phys.*, 90, 2121, 2001.
3. Gusev, E.P., Narayanan, V., and Frank, M.M., Advanced high-*k* dielectric stacks with poly-Si and metal gates: Recent progress and current challenges, *IBM J. Res. Dev.*, 50, 387, 2006.
4. Wallace, R.M. and Wilk, G.D., High-*k* dielectric materials for microelectronics, *Crit. Rev. Solid State Mater. Sci.*, 28, 231, 2003.
5. Wilk, G.D., Wallace, R.M., and Anthony, J.M., High-*k* gate dielectrics: Current status and materials properties considerations, *J. Appl. Phys.*, 89, 5243, 2001.
6. Gusev, E., *Defects in Advanced High-k Dielectric Nano-Electronic Semiconductor Devices*, Springer, Dordrecht, the Netherlands, 2006.
7. Bersuker, G. et al., Mechanism of charge trapping reduction in scaled high-*k* gate stacks, in *Defects in Advanced High-k Dielectric Nano-Electronic Semiconductor Devices*, Gusev, E., Ed. Springer, Dordrecht, the Netherlands, 2006, p. 227.

8. Shluger, A.L. et al., *Models of Defects in Wide-Gap Oxides: Perspective and Challenges*, Elsevier, Amsterdam, 2003, p. 151.
9. Kresse, G. and Furthmüller, J., Efficiency of ab-initio total energy calculations for metals and semiconductors using a plane-wave basis set, *Comput. Mater. Sci.*, 6, 15, 1996.
10. Segall, M.D. et al., First-principles simulation: Ideas, illustrations and the CASTEP code, *J. Phys. Condens. Matter*, 14, 2717, 2002.
11. ABINIT software code. Available at: www.abinit.org.
12. CPMD software code. Available at: www.cpmd.org.
13. Demkov, A.A. et al., Density functional theory of high-*k* dielectric gate stacks, *Microelectron. Reliab.*, 47, 686, 2007.
14. Gavartin, J.L. and Shluger, A.L., Modeling $HfO_2/SiO_2/Si$ interface, *Microelectron. Eng.*, 84, 2412, 2007.
15. Robertson, J., High dielectric constant gate oxides for metal oxide Si transitors, *Rep. Prog. Phys.*, 69, 327, 2006.
16. Gavartin, J.L. et al., The role of nitrogen-related defects in high-*k* dielectric oxides: Density-functional studies, *J. Appl. Phys.*, 97, 053704, 2005.
17. Xiong, K. and Robertson, J., Point defects in HfO_2 high *K* gate oxide, *Microelectron. Eng.*, 80, 408, 2005.
18. Onida, G., Reining, L., and Rubio, A., Electronic excitations: Density-functional versus many-body Green's-function approaches, *Rev. Mod. Phys.*, 74, 601, 2002.
19. Botti, S. et al., Time-dependent density-functional theory for extended systems, *Rep. Prog. Phys.*, 70, 357, 2007.
20. Rushton, P.P., Tozer, D.J., and Clark, S.J., Nonlocal density-functional description of exchange and correlation in silicon, *Phys. Rev. B*, 65, 235203, 2002.
21. Chu, S.I., Recent development of self-interaction-free time-dependent density-functional theory for nonperturbative treatment of atomic and molecular multiphoton processes in intense laser fields, *J. Chem. Phys.*, 123, 062207, 2005.
22. Todorova, T. et al., Molecular dynamics simulation of liquid water: Hybrid density functionals, *J. Phys. Chem. B*, 110, 3685, 2006.
23. Becke, A.D., A new mixing of Hartree–Fock and local density-functional theories, *J. Chem. Phys.*, 98, 1372, 1993.
24. Saunders, V. et al., *CRYSTAL2003 User's Manual*, University of Torino, Torino, 2003.
25. Cora, F. et al., The performance of hybrid density functionals in solid state chemistry, in *Principles and Applications of Density Functional Theory in Inorganic Chemistry II*, Springer, Berlin/Heidelberg, 2004, Vol. 113, p. 171.
26. Foster, A.S. et al., Vacancy and interstitial defects in hafnia, *Phys. Rev. B*, 65, 174117, 2002.
27. Foster, A.S., Shluger, A.L., and Nieminen, R.M., Mechanism of interstitial oxygen diffusion in hafnia, *Phys. Rev. Lett.*, 89, 225901, 2002.
28. Gavartin, J.L. et al., Ab initio modeling of structure and defects at the HfO_2/Si interface, *Microelectron. Eng.*, 80, 412, 2005.
29. Demkov, A.A., Thermodynamic stability and band alignment at a metal-high-*k* dielectric interface, *Phys. Rev. B*, 74, 085310, 2006.
30. Xiong, K. et al., Defect energy levels in HfO_2 high-dielectric-constant gate oxide, *Appl. Phys. Lett.*, 87, 183505, 2005.
31. Broqvist, P. and Pasquarello, A., Oxygen vacancy in monoclinic HfO_2: A consistent interpretation of trap assisted conduction, direct electron injection, and optical absorption experiments, *Appl. Phys. Lett.*, 89, 262904, 2006.
32. Gavartin, J.L. et al., Negative oxygen vacancies in HfO_2 as charge traps in high-*k* stacks, *Appl. Phys. Lett.*, 89, 082908, 2006.
33. Ramo, D.M. et al., Spectroscopic properties of oxygen vacancies in monoclinic HfO_2 calculated with periodic and embedded cluster density functional theory, *Phys. Rev. B*, 75, 205336, 2007.
34. Filippetti, A., Fiorentini, V., and Lopez, G.M., Electronic structure of defects in dielectrics with electronic correlation, *Electrochem. Soc. Trans.*, 3, 267, 2006.
35. Houssa, M., *High-k Dielectrics*, Institute of Physics Publishing, Bristol, 2004, p. 597.

36. Baraff, G.A., Kane, E.O., and Schlüter, M., Theory of the silicon vacancy: An Anderson negative-*U* system, *Phys. Rev. B*, 21, 5662, 1980.
37. Van de Walle, C.G. and Neugebauer, J., First-principles calculations for defects and impurities: Applications to III-nitrides, *J. Appl. Phys.*, 95, 327, 2006.
38. Sayan, S. et al., Band alignment issues related to HfO_2/SiO_2/p-Si gate stacks, *J. Appl. Phys.*, 96, 7485, 2004.
39. Takeuchi, H., Ha, D., and King, T.-K., Observation of bulk HfO_2 defects by spectroscopic ellipsometry, *J. Vac. Sci. Technol. Sci. Technol. A*, 22, 1337, 2004.
40. Pruneda, J.M. and Artacho, E., Energetics of intrinsic point defects in $ZrSiO_4$, *Phys. Rev. B*, 71, 094113, 2005.
41. Stoneham, M. et al., The vulnerable nanoscale dielectric, *Phys. Status Solidi (a)*, 204, 653, 2007.
42. Xiong, K. et al., Defect states in the high-dielectric-constant gate oxide $HfSiO_4$, *J. Appl. Phys.*, 101, 024101, 2007.
43. Sushko, P.V. et al., Oxygen vacancies in amorphous silica: Structure and distribution of properties, *Microelectron. Eng.*, 80, 292, 2005.
44. Gavartin, J.L. et al., Polaron-like charge trapping in oxygen deficient and disordered HfO_2: Theoretic insight, in Physics and Technology of High-*k* Dielectrics 4, Kar, S. et al., Eds. Electrochemical Society, Pennington, NJ, 2006, p. 277.
45. Gavartin, J.L. and Shluger, A.L., Ab initio modeling of electron–phonon coupling in high-*k* dielectrics, *Phys. Status Solidi C*, 3, 3382, 2006.
46. Stoneham, A.M. et al., Trapping, self-trapping and the polaron family, *J. Phys. Condens. Matter*, 19, 255208, 2007.
47. Ramo, D.M. et al., Intrinsic and defect-assisted trapping of electrons and holes in HfO_2: An ab initio study, *Microelectron. Eng.*, 84, 2362, 2007.
48. Ramo, D.M. et al., Theoretical prediction of intrinsic self-trapping of electrons and holes in the monoclinic HfO_2, *Phys. Rev. Lett.*, 99, 155504, 2007.
49. Diebold, A.C. et al., Characterization and production metrology of thin transistor gate oxide films, *Mater. Sci. Semicond. Process.*, 2, 103, 1999.
50. Frank, M.M. et al., HfO_2 and Al_2O_3 gate dielectrics on GaAs grown by atomic layer deposition, *Appl. Phys. Lett.*, 86, 152904, 2005.
51. Nguyen, N.V. et al., Sub-bandgap defect states in polycrystalline hafnium oxide and their suppression by admixture of silicon, *Appl. Phys. Lett.*, 87, 192903, 2005.
52. Walsh, S. et al., Process-dependent defects in Si/HfO_2/Mo gate oxide heterostructures, *Appl. Phys. Lett.*, 90, 052903, 2007.
53. Bersuker, G. et al., The effect of interfacial layer properties on the performance of Hf-based gate stack devices, *J. Appl. Phys.*, 100, 094108, 2006.
54. Sayan, S. et al., Effect of nitrogen on band alignment in HfSiON gate dielectrics, *Appl. Phys. Lett.*, 87, 212905, 2005.
55. Afanas'ev, V.V. and Stesmans, A., Spectroscopy of electron states at interfaces of (100) Ge with high-kappa insulators, *Mater. Sci. Semicond. Process.*, 9, 764, 2006.
56. Afanas'ev, V.V. et al., Band alignment between (100) Si and Hf-based complex metal oxides, *Microelectron. Eng.*, 80, 102, 2005.
57. Miyazaki, S. et al., Chemical and electronic structure of ultrathin zirconium oxide films on silicon as determined by photoelectron spectroscopy, *Solid State Electron.*, 46, 1679, 2002.
58. Yamaoka, M., Murakami, H., and Miyazaki, S., Diffusion and incorporation of Zr into thermally grown SiO_2 on Si(100), *Appl. Surf. Sci.*, 216, 223, 2003.
59. Cho, Y.J. et al., Spectroscopic ellipsometry characterization of high-*k* dielectric HfO_2 thin films and the high-temperature annealing effects on their optical properties, *Appl. Phys. Lett.*, 80, 1249, 2002.
60. Kirsch, P.D. et al., Nucleation and growth study of atomic layer deposited HfO_2 gate dielectrics resulting in improved scaling and electron mobility, *J. Appl. Phys.*, 99, 023508, 2006.
61. Kerber, A. et al., Origin of the threshold voltage instability in SiO_2/HfO_2 dual layer gate dielectrics, *IEEE Electron Dev. Lett.*, 24, 87, 2003.

62. Bersuker, G. et al., Intrinsic threshold voltage instability of the HfO_2 NMOS transistors, *Proc. IEEE Intl. Reliab. Phys. Sympos.*, San Jose, CA, 2006, p. 179.
63. Heh, D. et al., Spatial distributions of trapping centers in HfO_2/SiO_2 gate stack, *IEEE Trans. Electron Dev.*, 54, 1338, 2007.
64. Young, C.D. et al., Electron trap generation in high-*k* gate stacks by constant voltage stress, *IEEE Trans. Dev. Mater. Reliab.*, 6, 123, 2006.
65. Campbell, J.P. et al., Observations of NBTI-induced atomic-scale defects, *IEEE Trans. Dev. Mater. Reliab.*, 6, 117, 2006.
66. Neugroschel, A. et al., An accurate lifetime analysis methodology incorporating governing NBTI mechanisms in high-k/SiO_2 gate stacks, *IEEE IEDM*, San Francisco, CA, 2006, p. 317.
67. Felix, J.A. et al., Total-dose radiation response of hafnium-silicate capacitors, *IEEE Trans. Nucl. Sci.*, 49, 3191, 2002.
68. Felix, J.A. et al., Effects of radiation and charge trapping on the reliability of high-kappa gate dielectrics, *Microelectron. Reliab.*, 44, 563, 2004.
69. Felix, J.A. et al., Radiation-induced charge trapping in thin Al_2O_3/SiO_xN_y/Si(100) gate dielectric stacks, *IEEE Trans. Nucl. Sci.*, 50, 1910, 2003.
70. Kang, A.Y., Lenahan, P.M., and Conley, J.F., The radiation response of the high dielectric-constant hafnium oxide/silicon system, *IEEE Trans. Nucl. Sci.*, 49, 2636, 2002.
71. Kang, A.Y., Lenahan, P.M., and Conley, J.F., Electron spin resonance observation of trapped electron centers in atomic-layer-deposited hafnium oxide on Si, *Appl. Phys. Lett.*, 83, 3407, 2003.
72. Lucovsky, G. et al., Differences between charge trapping states in irradiated nano-crystalline HfO_2 and non-crystalline Hf silicates, *IEEE Trans. Nucl. Sci.*, 53, 3644, 2006.
73. Ryan, J.T. et al., Identification of the atomic scale defects involved in radiation damage in HfO_2 based MOS devices, *IEEE Trans. Nucl. Sci.*, 52, 2272, 2005.
74. Zhou, X.J. et al., Bias-temperature instabilities and radiation effects in MOS devices, *IEEE Trans. Nucl. Sci.*, 52, 2231, 2005.
75. Zhou, X.J. et al., Effects of switched-bias annealing on charge trapping in HfO_2 gate dielectrics, *IEEE Trans. Nucl. Sci.*, 53, 3636, 2006.
76. Charge trapping in ultrathin hafnium dioxide based MOSFETs, *IEEE Trans. Nucl. Sci.*, 54, 1883, 2007.